ERDC MSRC

Major Shared Resource Center

ERDC MSRC/PET TR/00-20

A Parallel-Processing Coupled Wave/Current/Sediment Transport Model

by

David J. S. Welsh
Keith W. Bedford
Rong Wang
Ponnuswamy Sadayappan

18 May 2000

06h0092000

A Parallel-Processing Coupled Wave/Current/Sediment Transport Model

Dr. David J.S. Welsh and Dr. Keith W. Bedford
Dept. of Civil and Environmental Engineering and Geodetic Science
The Ohio State University

Rong Wang and Dr. Ponnuswamy Sadayappan
Dept. of Computer and Information Science
The Ohio State University

Abstract

Predictions of water elevations, currents, wave heights, and sediment transport are important inputs in the planning of military activities in the marine environment. Numerical models of marine circulation and wind-waves have traditionally been run separately, and sediment transport models have typically only considered current-induced transport, neglecting wave-induced transport. The significant interactions between circulation, wave, and sediment transport fields have been neglected due to the limitations of sequential computer systems. This report documents the coupling of advanced wave, circulation, and sediment transport models using a physically realistic combined bottom boundary layer model, parallel-processing strategies, and high performance computing facilities at the U.S. Army Engineer Research and Development Center. This work is an extension of previous research that coupled circulation and wave models at the air-sea boundary layer. The models used are the WAM wave model, the CH3D-SED circulation and sediment transport model, and the WCBL bottom boundary layer model. The coupled system has been named the COupled MArine Prediction System (COMAPS). The completed system has been deployed for the Adriatic Sea and results are presented for coupled and non-coupled hindcasts. The hindcasts indicate that the use of WCBL can cause increases in predicted suspended sediment concentrations on the order of 200 % in shallow water under the influence of large waves. WCBL also reduces wave heights in shallow water and significantly dampens storm surge activity. The simulation speed of COMAPS for different combinations of WAM, CH3D-SED, and WCBL processes is also discussed.

1. Introduction

The accurate prediction of sediment transport and suspended sediment concentrations are important issues for a number of military activities. These activities include navigation channel maintenance and dredged material disposal, and the prediction of submarine sediment clouds in which vessels and assault troops can elude detection. Both wave and current motions cause sediment transport and suspension, but in traditional models only current-induced effects have been considered. In coastal waters, wave effects become important and their inclusion can greatly improve the accuracy of sediment predictions. Physics representations of combined wave-current bottom boundary layers have been developed in the last two decades (Glenn and Grant, 1987, for example), but due to the performance limitations of sequential computer systems, coupled numerical simulations have been limited to simplified models or idealized wave and current fields.

The aim of this research was to couple advanced marine circulation, sediment transport, wave, and boundary layer models to take full advantage of the U.S. Army Engineer Research and Development Center Major Shared Research Center (ERDC MSRC) high performance computing facilities. A parallel-processing coupled system has been developed using the WAM wind-wave model, the CH3D-SED circulation and sediment transport model, and the WCBL wave-current boundary layer model. WCBL receives input fields of wave, current, and sediment properties from the WAM and CH3D-SED models. It then simulates a nonlinear, coupled bottom boundary layer, including sediment-induced stratification, and returns improved estimates of bottom shear stress and bottom roughness to CH3D-SED and bottom friction factor to WAM.

This research is an extension of the work documented in Welsh et al. (1999), where the WAM and CH3D models were coupled at the atmospheric boundary layer. The couplings described in Welsh et al. (1999) have been retained here. Briefly, CH3D supplies WAM with water surface currents and elevations, resulting in transient current- and depth-related wave refraction, transport of waves by currents, and modified wind input using the effective wind vector. In return, WAM supplies CH3D with wave-related wind stresses and radiation stresses, resulting in increased wind input due to a rougher water surface, plus a direct transfer of surface momentum between the wave and current motions. Lake Michigan hindcasts showed that the atmospheric boundary layer couplings affected surface currents and storm surges on the order of 20%, and wave heights on the order of 5%. These interactions are large enough to significantly influence the planning of military operations, and comparisons with storm surge and wave height data showed that error statistics improved when the couplings were added.

The WAM/CH3D-SED/WCBL modeling system, including both atmospheric and bottom boundary layer couplings, has been named the COupled MArine Prediction System (COMAPS).

2. Models used

The WAM and CH3D models are described in detail in Zhang et al. (1998). The SED model is described in detail in Welsh et al., (1999). Brief descriptions of these models are repeated below, along with extensive details of the WCBL model.

The WAM wind-wave model (WAMDI, 1988) predicts unsteady frequency-direction spectra of wave energy on a regular, spherical (longitude/latitude) grid. Significant wave heights, mean wave periods, and mean wave directions are calculated from the spectra. WAM cycle 4 (Gunther et al., 1992) is used here. This version is based on the wave action density conservation equation, in terms of frequencies relative to the local current, and includes advanced, “third-generation” physics (Komen et al., 1994) in the calculation of wind input, nonlinear wave-wave interaction, and dissipation source/sink terms.

The CH3D marine circulation model (Chapman et al., 1996) predicts unsteady three-dimensional current, temperature, and salinity fields, and two-dimensional water surface elevation fields. The model solves conservation equations for mass, momentum, thermal energy, and salinity using a curvilinear horizontal grid and a sigma-layer (terrain following) vertical grid. A mode-splitting solution technique is used in which external (barotropic; depth-averaged) motions and internal (baroclinic; depth-varying) motions are solved separately, allowing a longer baroclinic time-step.

The SED sediment tranport and concentration model predicts three-dimensional fields of sediment concentration for an arbitrary number of user-specified sediment size classes. In CH3D-SED (Spasojevic and Holly, 1994), the SED sediment calculations are fully integrated with the CH3D circulation calculations. The SED model accounts for erosion, deposition, and bedload transport in an active layer at the top of the bed, and also calculates suspended sediment transport. Sediment mass conservation equations are solved for each size class both in the active layer and at each CH3D-SED vertical sigma-layer. Each time-step, CH3D supplies SED with grids of water depths and currents. SED returns grids of modified depths and near-bottom water/sediment mixture densities.

The origins of the WCBL model lie with the wave-current boundary layer theory of Grant and Madsen (1979). This work addressed wave-dominated conditions and did not account for stratification due to suspended sediment. Glenn and Grant (1987) added the stratification effect, and Keen and Glenn (1998) extended the applicability of the theory to a wider range of wave-current regimes. The original WCBL code was written by Lee (1992), with the modifications of Keen and Glenn (1998) added for the COMAPS project.

The WCBL model uses two dimensionless shear velocities that represent the interacting effects of the wave and current boundary layers. The maximum combined shear velocity is given by

$$U_{*cw} = \left(\frac{f_{cw}}{2} U_b^2 \boldsymbol{a} \right)^{0.5}, \tag{1}$$

where U_b is the wave-induced orbital velocity at the top of the wave boundary layer, $\boldsymbol{a}$ is a dimensionless function that accounts for current effects, and f_{cw} is a combined wave-current friction factor calculated from a nonlinear, directional function of U_b, the near-bed current, and parameters describing the sediment size classes. The time-averaged shear velocity is given by

$$U_{*c} = \left(\frac{f_{cw}}{2} U_b^2 V_2 \right)^{0.5}, \tag{2}$$

where V_2 is another dimensionless function, similar to $\boldsymbol{a}$, first used in Grant and Madsen (1979). U_{*cw} and U_{*c} correspond to wave-current and current-only effects, respectively, with f_{cw}, $\boldsymbol{a}$, and V_2 accounting for the interactions between the boundary layers. The height of the wave boundary layer is calculated using

$$\boldsymbol{d}_w = \frac{2\boldsymbol{k} U_{*cw}}{\boldsymbol{w}}, \tag{3}$$

where $\boldsymbol{k}$ is the von Karman coefficient, (= 0.4), and $\boldsymbol{w}_p$ is a representative radian wave frequency, taken here to be the peak wave frequency. It should be noted that (1) and (2) are similar in form to the widely used Taylor drag law:

$$\frac{\boldsymbol{t}}{\boldsymbol{r}} = \left(C_d U^2\right)^{0.5}, \tag{4}$$

where $\boldsymbol{t}$ represents shear stress, $\boldsymbol{r}$ is the density of the medium, C_d is a drag coefficient, and U is a velocity.

WCBL uses (1) – (3) in the calculation of the apparent bottom roughness due to the combined boundary layer:

$$k_{bc} = k_b \left(30 \frac{\boldsymbol{d}_w}{k_b} \right)^{\left(1 - \frac{U_{*c}}{U_{*cw}}\right)}, \tag{5}$$

$$= k_b \left(30 \frac{\boldsymbol{d}_w}{k_b} \right)^{\left(1 - \left(\frac{V}{\boldsymbol{a}}\right)^{0.5}\right)}, \tag{6}$$

where k_b is the physical bottom roughness and

$$k_b = k_{bS} + k_{bR} + k_{bT} \tag{7}$$

with k_{bS} is a representative sediment grain size for the active layer of sediment transport; k_{bR} is related to ripple height and steepness; and k_{bT} represents roughness due to "breakoff" sediment transport in high-shear conditions. WCBL uses a moveable bed roughness theory to calculate k_{bR} and k_{bT} from U_{*cw} and sediment size class parameters. For large waves and small currents, function $V_2 \to 0$, while function $\boldsymbol{a} \to 1$. This means that (6) gives $k_{bc} \approx 30\boldsymbol{d}_w$, which is the roughness for a pure wave boundary layer. Conversely, for small waves and large currents, the ratio $\left(V_2/\boldsymbol{a}\right) \to 1$, and k_{bc} from (6) reverts to the current boundary layer roughness k_b.

The current profile for the combined boundary layer is

$$U(z) = \frac{U_{*c}}{\boldsymbol{k}} \left(\ln \frac{30z}{k_{bc}} \right) + \boldsymbol{ba} \ln \frac{z}{\boldsymbol{d}_w}, \tag{8}$$

where $\boldsymbol{b}$ is a constant.

The solution procedure in WCBL is:

1. Use the unstratified wave-current boundary layer theory of Keen and Glenn (1998) to iteratively calculate a representative boundary layer current, U_a. A known current, U_r, which applies at reference elevation Z_r, is used as the first guess for U_a.

2. Use the result from step 1. as the first guess for U_a in the stratified wave-current boundary layer calculations.
3. Evaluate functions V_2 and $\boldsymbol{a}$ using U_a, U_b, and $\Delta\boldsymbol{q}_{cw}$, the angle between the current and wave velocity vectors.
4. Estimate f_{cw}, then U_{*cw} and U_{*c} using (1), (2), and additional equations from Keen and Glenn (1998).
5. Calculate k_b using (7) and additional equations for k_{bR} and k_{bT}.
6. Calculate k_{bc} using (5).
7. Calculate U_r using (8), then apply a correction to account for stratification due to suspended sediment.
8. Compare U_r from step 7. to the known U_r to check for convergence. If convergence has not occurred, return to step 3.

The parallel-processing codes developed for this research use two different computational strategies. One-dimensional domain decomposition was used in CH3D-SED and WCBL. A pre-processor divides the grid into a user-specified number of horizontal blocks. Only the grid points that fall on water are used in the computation, so the number of rows per block must be varied to give good load balancing. A two-dimensional decomposition was not selected since it would have made good load balancing difficult to attain. During the CH3D-SED and WCBL simulations, the processors for neighboring blocks send each other updated arrays using calls to the Message Passing Interface (MPI) library of functions. A parallel version of WAM was obtained using the OpenMP library. More complete details of the parallelization strategies are contained in Welsh et al. (1999) and Bangalore et al. (1999).

3. Inter-model communication

The CH3D-SED and WAM models must wait while the WCBL model calculates the combined boundary layer parameters. WCBL is, therefore, called as a subroutine by each CH3D-SED process and uses the same domain decomposition as CH3D-SED. Communication between WAM and WCBL uses MPI calls between the WCBL master process and sequential-processing regions of the WAM code. The coupled system has been run on the SGI ORIGIN 2000 platform at ERDC MSRC.

Figure 1 illustrates the launching of a simple coupled simulation and the ensuing intra- and inter-model communications. In the job's main shell script, the number of WAM threads is set using the "MP_SET_NUMTHREADS" function. The number of CH3D-SED/WCBL processes is then set in the "mpirun" command, which launches the simulation. The arrows in figure 1 are color-coded to indicate the source of the arrays being passed. The colors blue, red, and fuchsia indicate arrays calculated in the CH3D-SED, WAM, and WCBL models, respectively. The CH3D-SED and WCBL master processes use MPI to communicate with their slave processes and make the conversions from blocked to domain-wide arrays, and vice-versa, that are a necessary stage of all data exchanges with WAM.

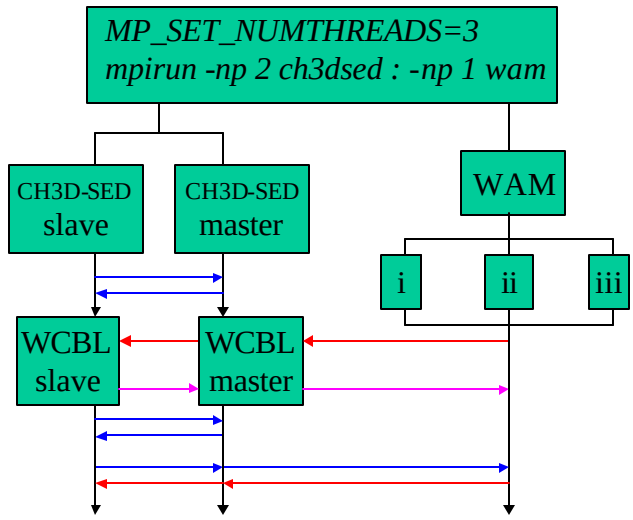

Figure 1. A simple example of parallel-processing and intra- and inter-model communication in the COMAPS coupled system

4. Inputs to the WCBL model

The WCBL model requires the following inputs from the other models in the coupled system:

<u>WAM</u>

- Near-bottom maximum horizontal excursion due to wave motion, A_b. Using linear wave theory, this is given by

$$A_b = \frac{H_s}{2\sinh\left(k_p h\right)}, \tag{9}$$

where k_p is the wave number at the spectral peak; h represents depth; and the significant wave height is calculated using the summation of wave energy in frequency-direction space:

$$H_s = 4\left[\sum E(\boldsymbol{w},\boldsymbol{q})\Delta\boldsymbol{w}\Delta\boldsymbol{q}\right]^{0.5}. \tag{10}$$

- Near-bottom maximum wave-induced velocity, U_b. Using linear theory, this is given by multiplying A_b by $\boldsymbol{w}_p$, the peak frequency of the wave spectrum.

- Mean wave direction, $\boldsymbol{q}_w$, which is calculated from the wave spectrum using energy-weighting.

CH3D

- The current, U_r, and current direction, $\boldsymbol{q}_r$, at a reference elevation, plus the reference elevation itself, z_r. The mid-point of the lowest CH3D sigma layer is used for z_r, and U_r and $\boldsymbol{q}_r$ are found using the velocity components calculated at that location.

SED

- The user-input specific weight of sediment grains, $\boldsymbol{g}_s$, which is generally 2.65.
- The grain size diameter for each user-specified sediment size class, $D(n)$.
- The volume-fraction concentration at the reference elevation for each size class, $C_{vr}(n)$. SED calculates mass-fraction concentrations, which are converted to $C_{vr}(n)$ by dividing by $\boldsymbol{g}_s$.
- The fiftieth percentile (by mass) grain size for the active layer of bedload transport, D_{50}. This is found using the active layer size class distributions calculated in SED and the $D(n)$ values.

5. Use of the WCBL results

The results from WCBL are used in the other models in the following manner:

WAM

- The combined wave-current friction factor, f_{cw}, is used in WAM in the calculation of the bottom friction energy dissipation rates. The standard WAM algorithm is (Shemdin, 1978):

$$S_{bf}(\boldsymbol{w},\boldsymbol{q}) = -C_f \frac{k}{\sinh(2kh)} E(\boldsymbol{w},\boldsymbol{q}), \tag{11}$$

where C_f is a friction coefficient which is set to 0.0077 m/s; wave number, k, is a function of $\boldsymbol{w}$ and h; and g represents gravitational acceleration. Komen et al. (1994; pp. 161-164) start from first principles and use a Taylor drag law form to derive an alternative expression:

$$S_{bf}(\boldsymbol{w},\boldsymbol{q}) = -2C_d U_{rms}^b \frac{k}{\sinh(2kh)} E(\boldsymbol{w},\boldsymbol{q}), \tag{12}$$

where C_d is a drag coefficient and U^b_{rms} is the root mean square near-bottom velocity due to the $E(\boldsymbol{w},\boldsymbol{q})$ wave component. Comparing (11) and (12) gives $C_f = 2C_d U^b_{rms}$. The drag law calculations in WCBL use $f_{cw}/2$ rather than the more standard C_d. It follows that the combined friction factor can be used in WAM in the following modified bottom friction algorithm:

$$S_{bf}(\boldsymbol{w},\boldsymbol{q}) = -f_{cw} U^b_{rms} \frac{k}{\sinh(2kh)} E(\boldsymbol{w},\boldsymbol{q}), \tag{13}$$

with linear theory, for a monchromatic wave component, giving

$$U^b_{rms} = \left[\frac{4}{\sqrt{2}\boldsymbol{p}} \frac{E(\boldsymbol{w},\boldsymbol{q})\Delta\boldsymbol{w}\Delta\boldsymbol{q}}{\sinh(kh)} \boldsymbol{w} \right]^{0.5}. \tag{14}$$

<u>CH3D-SED</u>

- The combined wave-current bottom shear velocity, U_{*cw}, is used to replace the current-induced bottom shear velocity calculated in CH3D-SED from a standard Taylor drag law, $U_{*c} = \sqrt{C_b} U_r$, where the bottom drag coefficient, C_b, is a user-specified constant. When coupling is switched on, U_{*cw} is, therefore, used in the CH3D x- and y-momentum equations and the SED calculations of bottom shear stress and near-bottom concentrations.

6. Adriatic Sea hindcasts

The COMAPS system has been deployed for the Adriatic Sea. A bathymetry grid comprised of 5-minutes longitude by 5-minutes latitude cells was downloaded from the "Data Warehouse" at the Naval Oceanographic Office web site (http://www.navo.navy.mil/newpage/index4.htm). The grid was used directly in WAM, and converted to the equivalent Cartesian coordinate grid for use in CH3D-SED. The grid contains 97 computational cells in the longitudinal direction and 73 cells in the latitudinal direction; the CH3D-SED cells vary in size, but are on the order of 10 km (x-direction) by 7 km (y-direction). The WAM deployment uses 25 frequency bins and 24 directional bins. The CH3D-SED vertical grid uses 20 regularly spaced sigma layers. A contour plot of the grid bathymetry is shown is figure 2. It should be noted that Ionian Sea grid cells were replaced by land to eliminate unnecessary computation.

Adriatic Sea hindcasts were performed for the period 2/1/99, 0 UTC to 2/8/99, 0 UTC. Dr. Rich Hodur of the Naval Research Laboratory, Monterey provided wind stress fields for this period. The fields were calculated by the Mediterranean Sea deployment of the U.S. Navy COAMPS atmospheric circulation model (Hodur, 1993). Adriatic Sea 5-minute wind fields were derived from the COAMPS 27-km Lambert Conformal grid using rotational and scale factor conversions, followed by interpolation. The hindcast period was selected due to strong wind and wave activity. Throughout the period, wind directions were typically northeasterly. Wind stresses

were highest during the first 36 hours of the period and tended to be largest in the northern part of the Adriatic. The hour-12 (2/1/99, 12 UTC) wind stress field is shown in figure 3. This field contained the highest stresses of all. The maximum stress noted on the figure converts to a 10-m wind velocity on the order of 30 m/s.

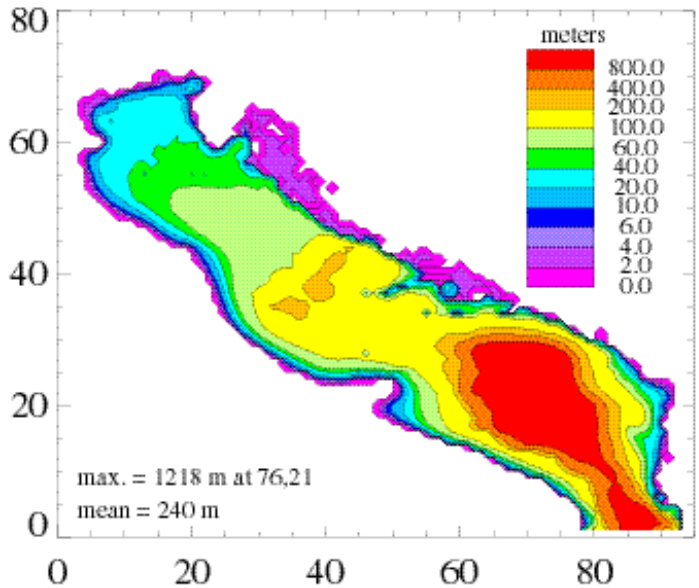

Figure 2: Depth contours and computational cell numbers for the 5-minute Adriatic Sea grid

Quiescent initial conditions were used for WAM waves and CH3D currents. In CH3D, initial temperature and salinity values were set to 4°C and 35 ppm at all grid points. At the open boundary at the southern end of the grid, a diurnal tidal boundary condition was imposed, with an amplitude of 1 m. Three sediment size classes were specified in SED, corresponding to typical sand, silt, and clay grains. Initial suspended sediment concentrations were set to zero. The initial (mass fraction) distribution of sediment sizes in the SED active and sub-stratum layers was set to 0.50:0.25:0.25 for the sand, silt, and clay classes, respectively. These are simplistic initial and tidal conditions, but they are sufficiently representative that they do not obscure the impacts of the model couplings in COMAPS. Detailed observational or hindcast data sets were not available for public domain use.

Hindcasts were performed for no model coupling (“0-way”); two-way atmospheric boundary layer coupling only, with WCBL switched off (“2-wayA”); and two-way atmospheric and bottom boundary layer coupling (“2-wayB”). A coupling frequency of 2 minutes was used in the coupled hindcasts. Comparisons of the predictions from the three sets of hindcasts are given below. These comparisons show the impacts of the couplings in COMAPS. Adriatic Sea data was not available for evaluation of the benefit of the couplings, but the comparative error statistics included in Welsh et al. (2000) confirm the benefit of the atmospheric boundary layer couplings in Lake Michigan hindcasts. Bottom boundary layer coupling was not included in the Lake Michigan study. It is, therefore, the focus of the following comparisons.

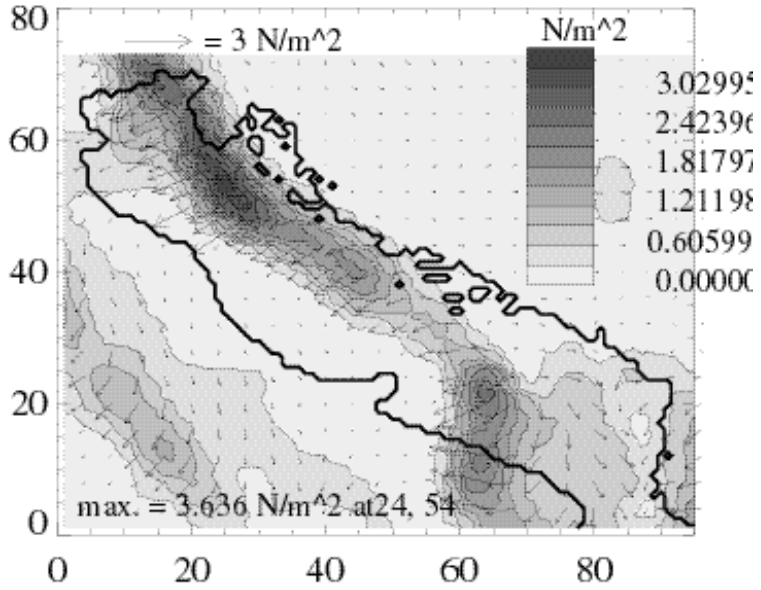

Figure 3: Wind stress contours and vectors for the 5-minute Adriatic Sea grid at hindcast hour-12

Results will be shown for hour-12 of the hindcast period since this time corresponded to the highest storm activity. This translates to the period of greatest risk for marine operations, and the largest wave, current, storm surge, and sediment transport effect. The coupling effects at hour-12 are also easy to see and are representative in nature.

Figure 4 shows contours of the shear velocities calculated in CH3D-SED for hour-12 of the 2-wayB hindcast. In the 2-wayB run, these shear velocities are replaced by the WCBL shear velocities shown in figure 5. It should be noted that values greater than 998.0 in figures 5 and 8 correspond to the regions where WCBL was unable to converge on a solution. In most cases this occurs when the near-bottom current is much greater than the near-bottom wave-induced velocity, resulting in a violation of model assumptions. This tends to happen in the Adriatic Sea where water depths are greater than 100 m, meaning that wave effects at the bed are negligible and WCBL is not required. WCBL also has convergence problems in very shallow water, as can be seen in Adriatic Sea regions where the depth is less than 4 m. This problem could be related to the increasing inaccuracy of linear wave theory as depths are reduced. When WCBL cannot converge, the original CH3D-SED shear velocities and WAM friction coefficient are used.

Comparing figures 4 and 5, it can be seen that CH3D-SED and WCBL shear velocities are similar in water depths greater than 60 m (refer to figure 2). This makes sense, as the wave boundary layer will be minimal. As depths fall, however, and wave effects become significant, the WCBL shear velocities become much larger. In water depths less than 20 m, the WCBL shear velocities are generally an order of magnitude greater than the CH3D-SED values. In certain shallow water locations, the ratio of shear velocities reaches two orders of magnitude. This level of increase seems excessive, and is under investigation. Another cause for concern is the horizontal band of high shear near the 20th row of cells in figure 4. There is no physical

reason for this feature and it appears to be related to the border between two grid blocks in the domain decomposition. Evidently, the master process (which made calculations up to row 21 in this case) is not correctly passing block-overlap values onto the relevant slave process. This issue is also being investigated.

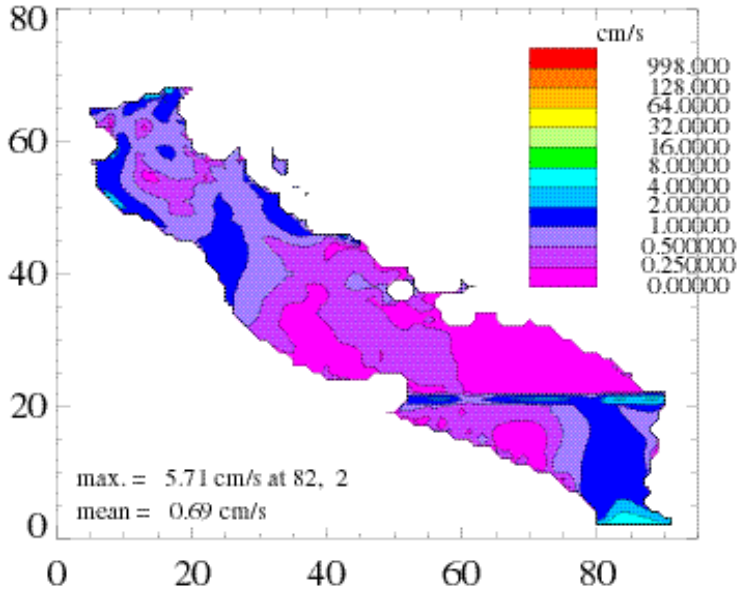

Figure 4: CH3D-SED shear velocities at hour-12 for the two-way coupling (WCBL on) hindcast

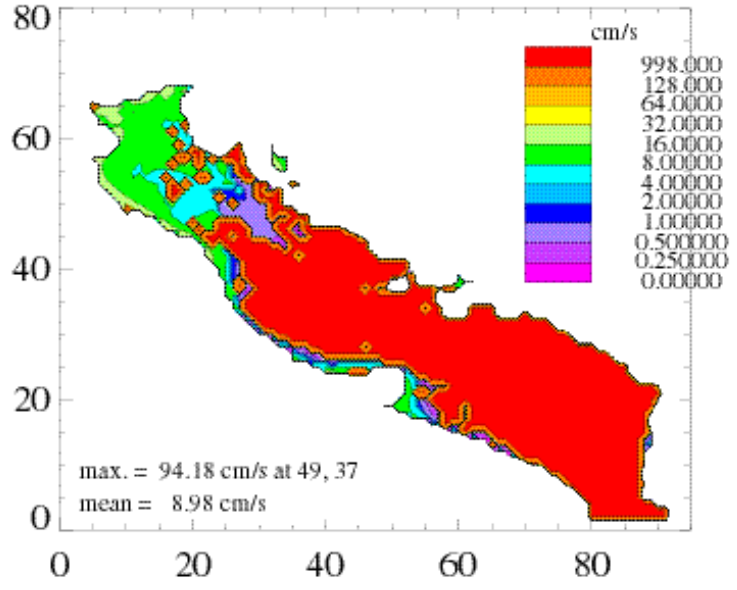

Figure 5: WCBL shear velocities at hour-12 for the two-way coupling (WCBL on) hindcast

Figures 6 and 7 show contours of the clay size class concentration at the lowest sigma layer at hour-12 of the 0-way and 2-wayB hindcasts. The concentrations for the 2-wayA hindcast are similar to those of the 0-way hindcast. Comparing figures 6 and 7, one can see that the enhanced WCBL shear velocities result in larger sediment concentrations, as one would expect. The increase only occurs in the regions where WCBL reached convergence, of course. The increase in sediment concentration is not as dramatic as the increase in shear-velocity. The typical increase is on the order of 200 %. This seems qualitatively reasonable, as large waves in shallow water (refer to figure 9 below) are likely to generate more sediment transport than the local currents. Excessive increases in concentration are seen in the very shallow regions where shear velocity increases were unreasonably large. The band of high concentration close to row 20 in figure 7 is due to the band of erroneous high shear velocities discussed above.

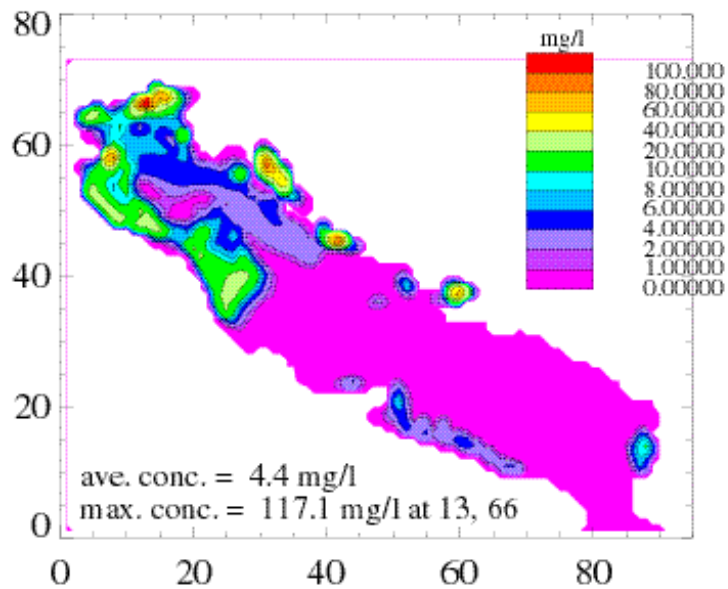

Figure 6: Clay concentrations in the lowest sigma layer at hour-12 of the no-coupling hindcast

Figure 8 shows the hour-12 ratio of the friction coefficient, C_f, from WCBL to the standard WAM C_f, which is 0.0077 m/s. Based on equations (11) and (13), the WCBL C_f is calculated in WAM by multiplying f_{cw} from WCBL by an energy-weighted U^b_{rms}. The deep water and very shallow water regions in which WCBL did not converge are again obvious in figure 8. It is interesting to note that the C_f ratio varies from approximately 0.1 up to 1.63, moving from deep water to very shallow water. This means that the WCBL C_f varies in a similar fashion, which is qualitatively reasonable since U^b_{rms} will increase in shallower water, C_d is likely to increase with U^b_{rms}, and $C_f = 2C_d U^b_{rms}$ (refer to section 5). The constant WAM C_f is in fact unreasonable.

Figure 9 shows significant wave height contours and vectors at hour-12 of the 0-way hindcast. The vector lengths are scaled with significant wave height and are aligned with mean wave direction. The wave vectors are closely aligned with the wind stress vectors in figure 3 and wave

heights are largest downwind of the highest wind stress regions. This illustrates fetch-limited growth, with wave heights then falling in shallow water as bottom friction increases.

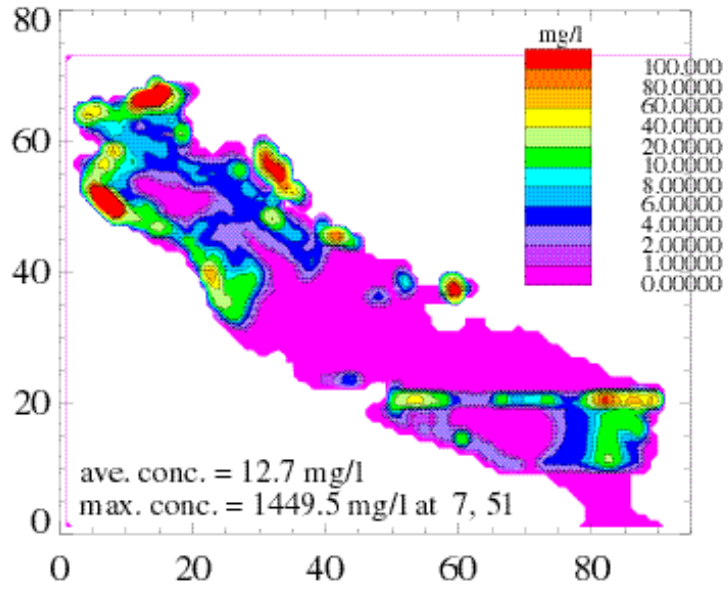

Figure 7: Clay concentrations in the lowest sigma layer at hour-12 of the two-way coupling (WCBL on) hindcast

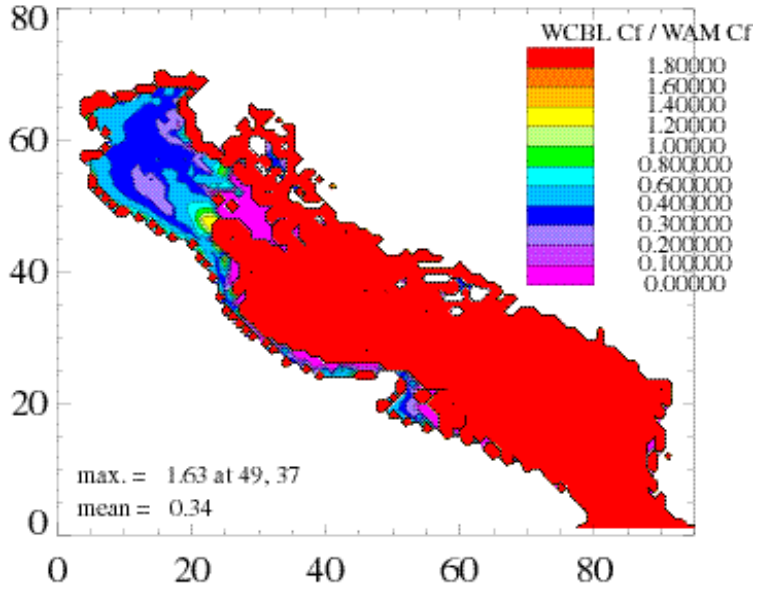

Figure 8: The ratio of WCBL friction coefficient to WAM friction coefficient at hindcast hour-12

Figure 10 shows the difference in significant wave height between the 2-wayA and 0-way hindcasts at hour-12. This indicates the impact of the atmospheric boundary layer (ABL)

couplings. The coupling effects are clearly most significant in the northern part of the sea, where wind stress, wave heights, and surface currents reach their maxima. There are areas where the significant wave height is affected +/- 10%. The changes are mainly due to modified effective wind vectors, due to wave propagation by currents. Due to the influences of bathymetry and the Coriolis force, surface currents are not always aligned with wind stresses (refer to figure 12), resulting in regions of both reduced and increased wind input and wave growth.

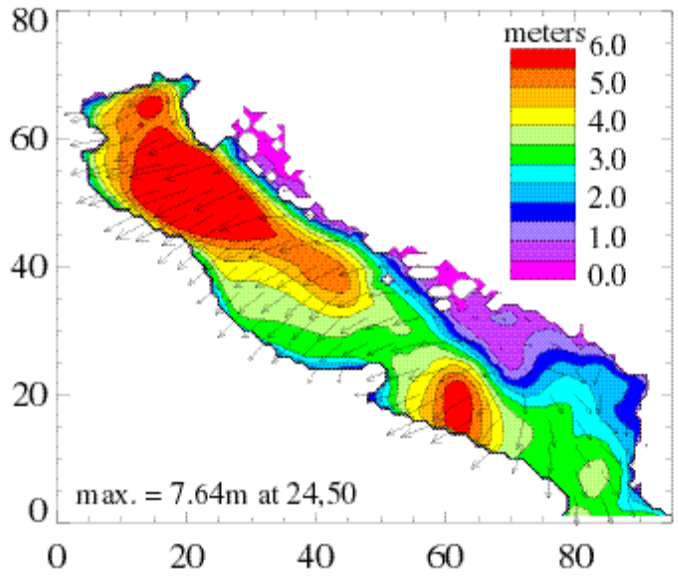

Figure 9: Significant wave height at hour-12 of the two-way coupling (WCBL off) hindcast

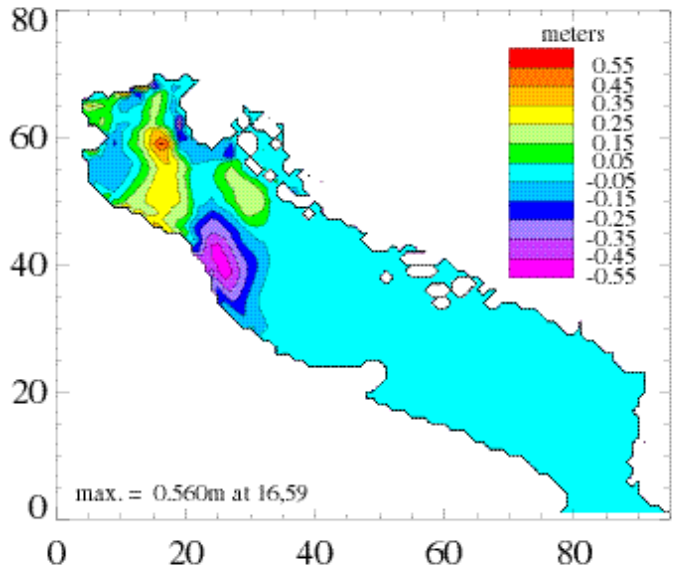

Figure 10: Significant wave height difference at hour-12 between the two-way coupling (WCBL off) and no coupling hindcasts

Figure 11 shows the difference in significant wave height between the 2-wayB and 2-wayA hindcasts at hour-12. This indicates the impact of the bottom boundary layer (BBL) couplings. The influence of the BBL couplings on wave heights is clearly much less than that of the ABL couplings. There are a few small regions where the use of WCBL has led to small reductions in wave height. Most notably, the increased bottom friction (refer to figure 8) in the region of grid point (25,45) causes reduced downwind wave heights, at around (25,40).

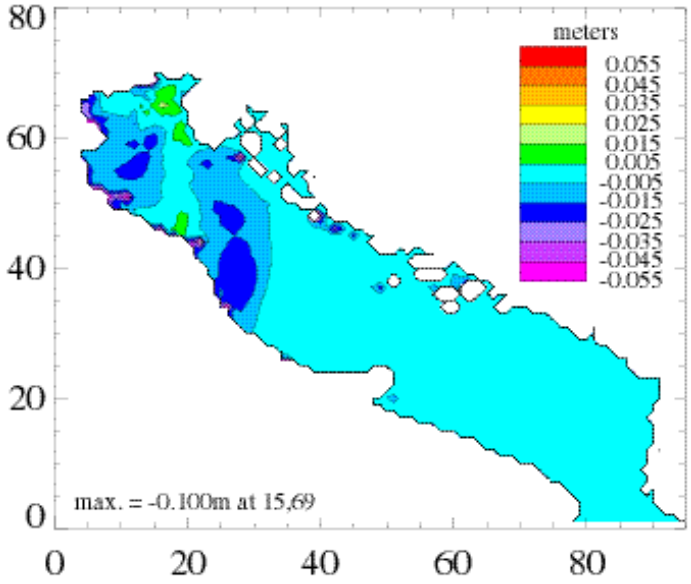

Figure 11: Significant wave height difference at hour-12 between the two-way coupling (WCBL on) and two-way coupling (WCBL off) hindcasts

Figure 12 shows water elevation contours and surface current vectors at hour-12 of the 2-wayA hindcast. The scale of the vector lengths is shown on the figure. The strong wind stresses have caused a 40 cm storm surge at the northwestern end of the sea and large surface current drive water to that location. The currents are generally aligned to the right of the wind vectors due to the Coriolis force. There is also a return flow evident along the northern half of the western shore.

Figure 13 shows the difference in water elevations between the 2-wayA and 0-way hindcasts at hour-12. The figure shows that the ABL couplings increase the storm surge by approximately 10 cm, or 33 % of the 0-way surge. This is caused by the transfer of energy to currents by radiation stress, plus the increased surface drag coefficient due to the presence of waves. These effects are discussed in detail in Welsh et al. (1999).

Figure 14 shows the difference in water elevations between the 2-wayB and 2-wayA hindcasts at hour-12. The use of WCBL reduces the storm surge by approximately 15 cm, or 50 % of the 0-way surge. The reduction is related to the increased bottom shear velocities supplied by WCBL. These correspond to increased bottom friction and, therefore, reduced velocities and water

transport. The magnitude of the surge reduction is rather high, which confirms that the WCBL shear velocities may be excessive in shallow water.

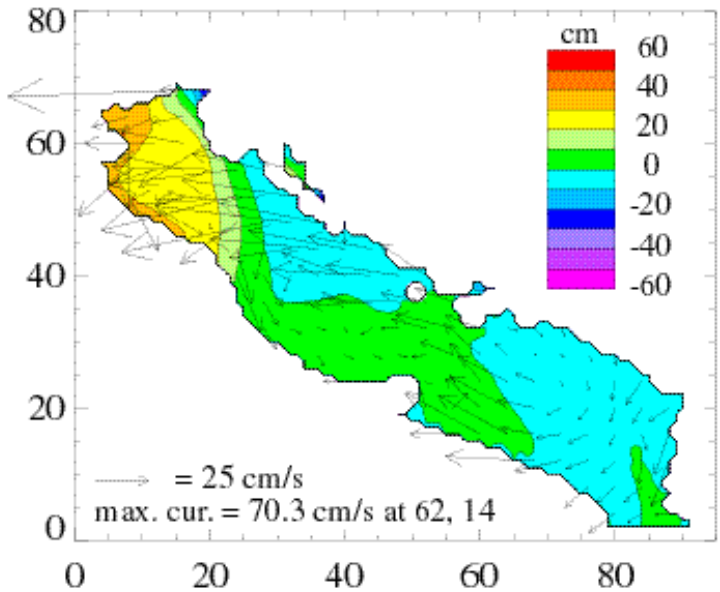

Figure 12: Water elevation contours and surface current vectors at hour-12 of the two-way coupling (WCBL off) hindcast

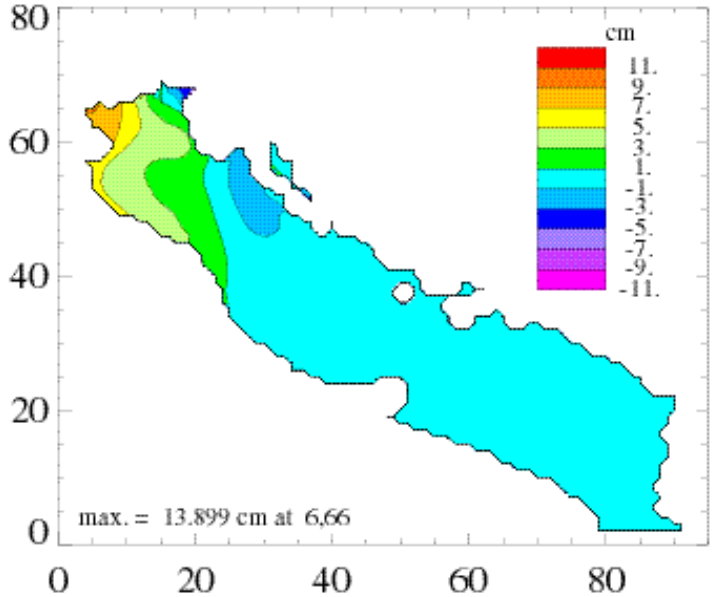

Figure 13: Water elevation difference between the two-way coupling (WCBL off) and no coupling hindcasts

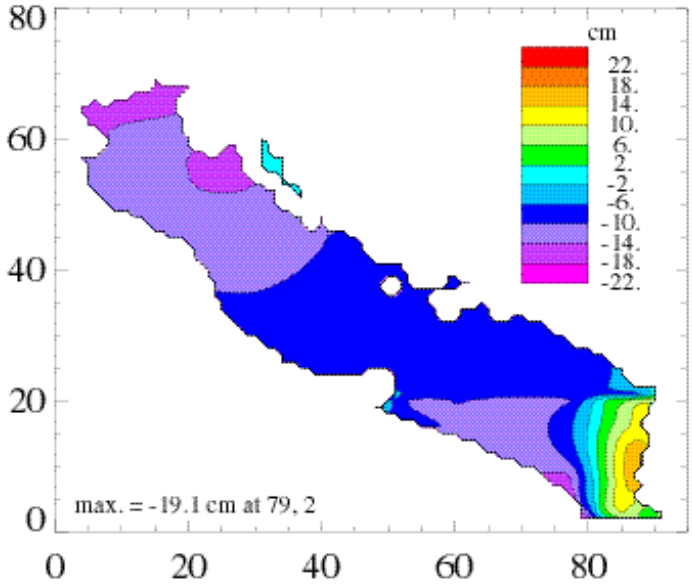

Figure 14: Water elevation difference between the two-way coupling (WCBL on) and two-way coupling (WCBL off) hindcasts

7. Computational performance results

The coupled system has been run on the SGI ORIGIN 2000 platform at ERDC MSRC. Simulation speed data has been obtained for three sets of runs:

1. number of CH3D-SED/WCBL processes held constant; number of WAM threads varied,
2. number of WAM threads held constant; number of CH3D-SED/WCBL processes varied,
3. total number of processes held constant, but distribution of processes between CH3D-SED/WCBL and WAM varied to identify the optimal distribution.

The latter set of tests most closely represents operational conditions. Figures 15 to 17 show performance results for the three sets of runs. It can be seen from figure 15 that the optimum simulation speed is reached with 6 WAM threads when the number of CH3D-SED/WCBL processes is fixed at 4. The variation of simulation time with the number of WAM threads shows that CH3D-SED is completing a time step more quickly than WAM. When only 2 CH3D-SED/WCBL processes are used, the simulation time is approximately constant until 8 or more WAM threads are used. The simulation time rises in figure 15 above 6 WAM threads because the number of computational cells per thread becomes small and communication overhead dominates. For a larger grid, both the rates and limit of performance improvement would be increased. In the coming year, the 5-minute Adriatic Sea grid will be replaced by a 2-minute grid. This will result in improved system scalability and more accurate predictions.

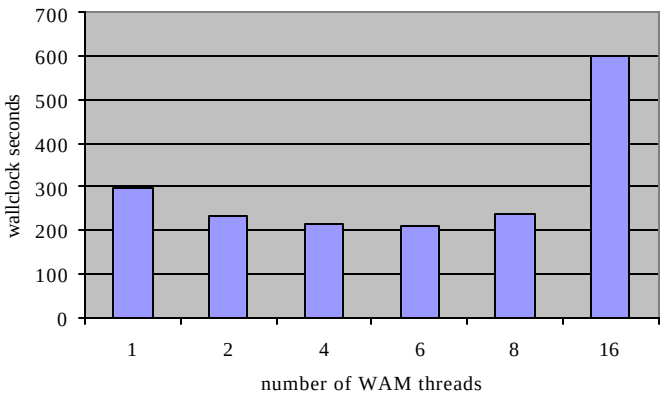

Figure 15: Wallclock time for 1 hour Adriatic Sea run using 4 CH3D-SED/WCBL processes and a varying number of WAM threads

Figure 16 shows that the simulation speed is approximately steady when 2 WAM threads are used with 8 or less CH3D-SED/WCBL processes. The reason for this is that CH3D-SED is completing a time step more quickly than WAM. When more than 8 CH3D-SED/WCBL processes are used, the level of communication overhead in CH3D-SED becomes excessive and simulation times increase. It is not clear why the simulation time falls moving from 10 to 16 CH3D-SED/WCBL processes. This could be a result of inaccurate timings, but each timing is based on an average of two runs. It is possible that cache-missing behavior is a factor.

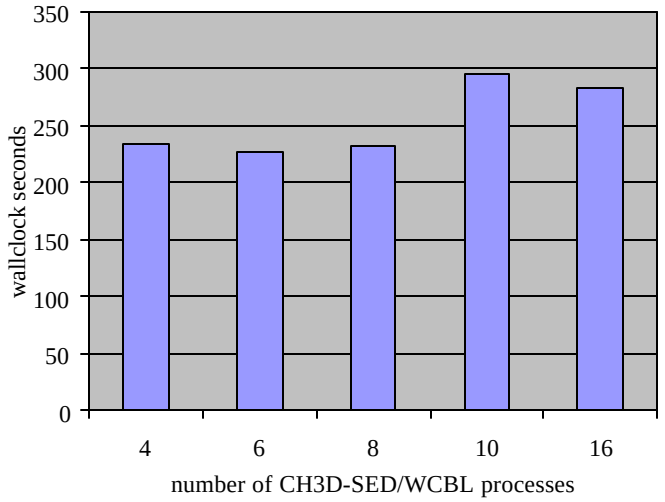

Figure 16: Wallclock time for 1 hour Adriatic Sea run using 2 WAM threads and a varying number of CH3D-SED/WCBL processes

Figure 17 shows that when 12 processors are to be used, optimum simulation speed is obtained with 8 CH3D-SED/WCBL processes and 4 WAM threads. For this distribution, CH3D-SED and WAM complete a time-step in approximately the same time. It should be noted, however, that two of the runs shown in figure 15 took less time than the fastest run in figure 17. This indicates that it isn't always best to use the total number of processors available if the total number of grid cells is relatively low.

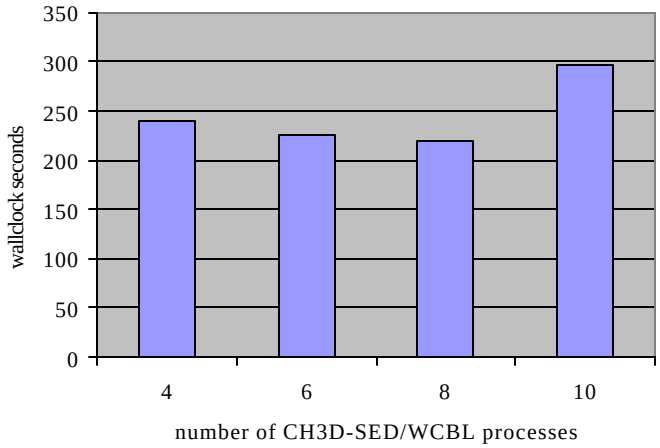

Figure 17: Wallclock time for 1 hour Adriatic Sea run using a fixed total of 12 processes/threads, but varying the numbers of CH3D-SED/WCBL processes and WAM threads

8. Conclusions and future research

Parallel-processing versions of the CH3D-SED marine circulation and sediment transport model, the WAM wind-wave model, and the WCBL bottom boundary layer model have been coupled, resulting in the COupled MArine Prediction System (COMAPS). The system includes couplings at the atmospheric and bottom boundary layers. The integration of WCBL was recently completed. The model simulates the nonlinear interaction of wave and current boundary layers and accounts for stratification due to suspended sediment. WCBL receives wave, current, and sediment information from the other models, then supplies CH3D-SED and WAM with combined shear velocity and friction factor arrays, respectively. These arrays are used to replace the models' standard formulations.

Adriatic Sea hindcasts have been performed for different levels of coupling. The hindcasts indicate that WCBL shear velocities are often an order of magnitude greater than the CH3D values when large waves are present in water depths less than 20 m. The resulting increases in suspended sediment concentrations can be more than 200%. While combined shear velocities are likely to become dominated by wave motion in shallow water, the observed levels of increase may be excessive. This issue is under investigation. WAM uses a fixed bottom friction coefficient, but WCBL was found to calculate friction coefficients up to 90% lower in deep water and 60% higher in very shallow water. This variation is at least qualitatively more reasonable. WCBL tends not to converge in water depths greater than 100 m and less than 4 m. This appears to be caused by violations of model assumptions; in deep water, wave-induced bottom stresses become negligible, and in very shallow water, linear wave theory loses validity. Where WCBL does not reach a solution, the standard CH3D-SED and WAM bottom boundary layers are used.

COMAPS has been run on the U.S. Army ERDC MSRC SGI ORIGIN 2000 computer and performance measures have been collected for various numbers of processors devoted to the three component models. Results indicate that the number of cells in the 5-minute Adriatic Sea grid is too low for a fair assessment of system scalability. System performance will be tested in the near future using a 2-minute Adriatic Sea grid.

In summary, hindcast analysis indicates that the predictions of the WCBL model vary in a realistic manner, but further work is required to improve quantitative accuracy. When this task is complete, it appears likely that the sophisticated physics and parallel-processing nature of COMAPS will allow timely generation of more accurate marine circulation, wave, and sediment transport predictions. This will result in a significant upgrade in the support of military operations.

Acknowledgment

This work was supported in part by a grant of HPC time from the DoD HPC Modernization Program.

References

Bangalore, P.V., Zhu, J., Huddleston, D., Skjellum, A., Welsh, D.J.S., Bedford, K.W., Wang, R. and Sadayappan, P., 1999. Parallelization of a coupled hydraulics and sediment transport model, *Technical Report ERDC MSRC/PET TR/99-23*, Mississippi State University and The Ohio State University. Prepared for the Department of Defense HPC Modernization Program.

Chapman, R.S., Johnson, B.H. and Vemulakonda, S.R., 1996. User's guide for the sigma stretched version of CH3D-WES; a three-dimensional numerical hydrodynamic and temperature model, *Technical Report HL-96-21*, U.S. Army Engineer Waterways Experiment Station, Vicksburg, MS.

Glenn, S.M. and Grant, W.D., 1987. A suspended sediment stratification correction for combined wave and current flows, *Journal of Geophysical Research*, **92**: 8244—8264.

Grant, W.D. and Madsen, O.S., 1979. Combined wave and current interaction with a rough bottom, *Journal of Geophysical Research*, **84**: 1797-1808.

Gunther, H., Hasselmann, S. and Janssen, P.A.E.M., 1992. The WAM model cycle 4, *Technical Report*, Deutsches KlimaRechenZentrum, Hamburg, Germany.

Hodur, R.M., 1993. Development and testing of the coupled ocean/atmosphere mesoscale prediction system (COAMPS), *NRL Memorandum Report 7533-93-7213*, Naval Research Laboratory, Monterey, CA.

Keen, T.R. and Glenn, S.M., 1998. Resuspension and advection of sediment during Hurricane Andrew on the Louisiana continental shelf, *Proceedings of the 5th International Conference on Estuarine and Coastal Modeling*, 481-494.

Komen, G.J., Cavalieri, L., Donelan, M., Hasselmann, K., Hasselmann, S. and Janssen, P.A.E.M., 1994. *Dynamics and Modelling of Ocean Waves*, Cambridge University Press, Cambridge, U.K.

Lee, J., 1992. An empirical relationship between the bed-load concentration and the excess shear stress in a wave-current boundary layer, *Master's Thesis*, The Ohio State University, Columbus, OH.

Shemdin, O.M., Hasselmann, K., Hsiao, S.V., and Herterich, K., 1978. Nonlinear and linear bottom interaction effects in shallow water, *Proceedings: NATO Symposium on Turbulent Fluxes through the Sea Surface*, Ile de Bendor, France.

Spasojevic, M. and Holly, M.J., 1994. Three dimensional numerical simulation of mobile-bed hydrodynamics, *Technical Report HL-94-2*, U.S. Army Engineer Waterways Experiment Station, Vicksburg, MS.

WAMDI, 1988. The WAM model – a third generation ocean wave prediction model, *Journal of Physical Oceanography* **18**: 1775-1810.

Welsh, D.J.S., Wang, R., Sadayappan, P., and Bedford, K.W., 1999. Coupling of marine circulation and wind-wave models on parallel platforms, *Technical Report ERDC MSRC/PET TR/99-22*, The Ohio State University, Columbus, OH. Prepared for the Department of Defense HPC Modernization Program.

Welsh, D.J.S., Bedford, K.W., Wang, R., and Sadayappan, P., 2000. Coupled hydrodynamic and wind-wave models of Lake Michigan. Submitted to the *Journal of Geophysical Research*.

Zhang, S., Welsh, D., Bedford, K., Sadayappan, P. and O'Neill, S., 1998. Coupling of circulation, wave and sediment models, *Technical Report ERDC MSRC/PET TR/98-15*, The Ohio State University, Columbus, OH. Prepared for the Department of Defense HPC Modernization Program.